THE JOURNAL OF PHYSICAL CHEMISTRY Letters

Letter

Cite This: J. Phys. Chem. Lett. 2019, 10, 4448−4454

pubs.acs.org/JPCL

Polariton-Assisted Cooperativity of Molecules in Microcavities Monitored by Two-Dimensional Infrared Spectroscopy

Zhedong Zhang,*[,†] Kai Wang,[†] Zhenhuan Yi,[†] M. Suhail Zubairy,[†] Marlan O. Scully,*[,†,‡,¶] and Shaul Mukamel*[,§]

[†]Institute for Quantum Science and Engineering, Texas A&M University, College Station, Texas 77843, United States

[‡]Quantum Optics Laboratory, Baylor Research and Innovation Collaborative, Waco, Texas 76704, United States

[¶]Department of Mechanical and Aerospace Engineering, Princeton University, Princeton, New Jersey 08544, United States

[§]Department of Chemistry, Department of Physics and Astronomy, University of California Irvine, Irvine, California 92697, United States

Supporting Information

ABSTRACT: Molecular polaritons created by the strong coupling between matter and field in microcavities enable the control of molecular dynamical processes and optical response. Multidimensional infrared spectroscopy is proposed for monitoring the polariton-assisted cooperative properties. The response of molecules to local fluctuations is incorporated and the full dynamics is monitored through the time- and frequency-resolved multidimensional signal. The cooperativity against solvent-induced disorder and its connection to the localization of the vibrational excitations are predicted. New insights are provided for recent 2DIR experiments on vibrational polaritons.

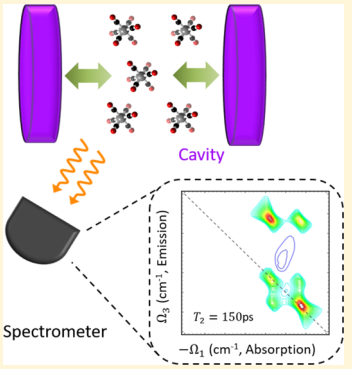

Microcavities offer a useful tool for controlling the coupling between matter and photons.[1−4] Strong coupling leads to a hybridization between material excitations and photons described through the joint matter-photon states known as polaritons. Molecular polaritons show an important feature of a mesoscopic coherence length on the material infrared (IR) polarization, in molecular vibrations.[5,6] Cavity polaritons lead to new dynamical properties with broad applications such as controllable energy transport in large molecules[7−11] and the manipulation of chemical reactivity.[12−15] Microcavities provide a powerful tool for studying strong radiation−matter coupling even for the vacuum field.[16−18] The cooperative interaction between many particles and cavity photons is of fundamental importance,[17,19,20] leading to many interesting phenomena, e.g., superradiance and subradiance in atoms and aggregates.[21−25] Such phenomena have been well studied in atomic systems. However, the situation becomes more complicated for molecules, due to nuclear motions.[26−28] For instance, the strong exciton−nuclei coupling leads to nonadiabatic dynamics which can change the energy surfaces.[29,30] This may cause inhomogeneous dephasing, which can compete with the cavity-mediated correlation between molecules.[31] Polaritons have been recently investigated in chromophore aggregates and organic molecules, showing the effects of vibrational transitions which considerably modify the photoluminescence spectra as well as chemical reactivity.[6,32−34] Despite these developments, the role of dephasing in the dynamics of molecules in microcavities remains an open issue.

Multidimensional spectroscopy provides an effective technique for studying polariton dynamics. This technique resolves the material dynamics by introducing several controllable time and frequency scales to reveal the information about material correlation functions, which is not possible through 1D techniques.[35−37] Coherent 2D spectra in semiconductor microcavities can provide experimental evidence of polariton−polariton interactions.[38,39] Recent technical advances have enabled the measurement of dipolar couplings in atomic gas by 2D technique with high precision.[40,41] 2D infrared spectra for molecular polaritons in $W(CO)_6$ were demonstrated where the pulse sequence was shined along the cavity axis and photon leakage from the cavity was detected.[42] Recent work has employed input−output theory to reproduce the polaritonic features observed in the experiments.[43]

In this Letter, we develop the third-order resonant infrared spectroscopy for the condensed-phase molecules in an infrared microcavity, incorporating the disorder caused by the solvent-induced fluctuations. Three time-ordered pulses are incident off the cavity axis which allows the collection of signal along the specific direction given by the phase matching condition.

Received: April 5, 2019
Accepted: July 13, 2019
Published: July 13, 2019

DOI: 10.1021/acs.jpclett.9b00979
J. Phys. Chem. Lett. 2019, 10, 4448−4454

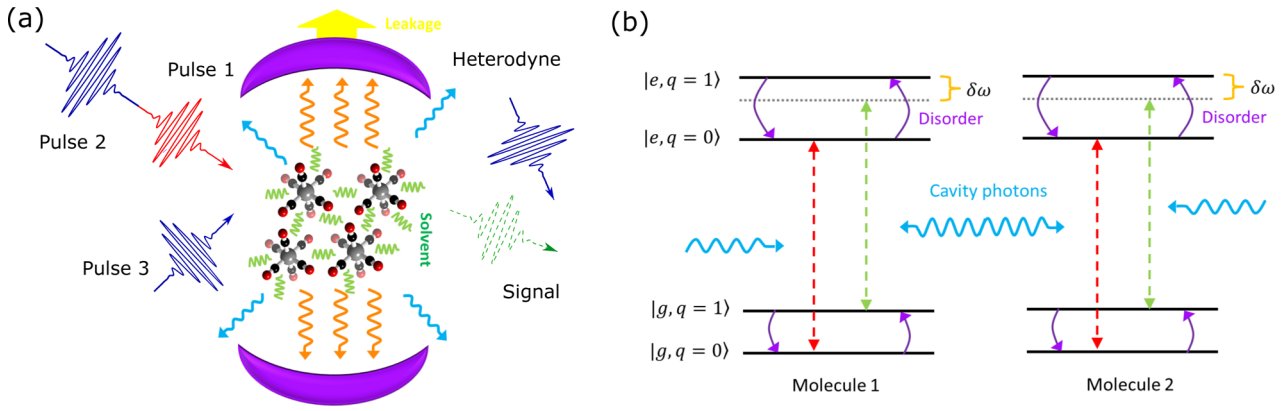

Figure 1. Schematic for 2D infrared spectroscopy of molecular polaritons. (a) Three time-ordered picosecond pulses incident off the cavity axis, with three controllable time delays T_1, T_2, T_3. (b) Level diagrams of molecules including disorder. Transition $|g, q = 0\rangle \leftrightarrow |e, q = 0\rangle$ (red dashed arrow) is resonant with photons while transition $|g, q = 1\rangle \leftrightarrow |e, q = 1\rangle$ (green dashed arrow) is off resonant with detuning $\delta\omega$ given by the vibration−solvent interaction $\delta\omega_j\eta_j|v_j\rangle\langle v_j|$ in eq 2; Disorder is caused by random transitions denoted by purple curved arrows.

We demonstrate the extra peaks resulting from the dynamical disorder that may erode the cooperativity between molecules. This resolves the *emitter dark states* (EDSs) attaching the oscillator strength by fluctuations that result in the weak coupling to cavity photons. Our results reveal the population transfer between polaritons and EDSs as well as polariton−polariton transfer. This offers new insights on recent experiments which demonstrated the coupling between EDSs and bright polaritons.[42] In addition, we study the role of localization and intermolecular coherence of vibrational excitations.

A group of two-level systems (TLS) coupled to the monochromatic electromagnetic (EM) wave is described by the Hamiltonian $H = \hbar(\omega_c a^\dagger a + \sum_{i=1}^N \omega_i|e_i\rangle\langle e_i| + \hbar\sum_{i=1}^N (\Omega_i e^{i\mathbf{k}\cdot\mathbf{r}_i}|e_i\rangle\langle g|a + \text{h. c.})$, whose eigenstates give the timed Dicke states found by Scully et al.[22]

$$|e_{\mathbf{k}}\rangle = \frac{1}{\sqrt{N}}\sum_{j=1}^{N} e^{i\mathbf{k}\cdot\mathbf{r}_j}|g_1, g_2, \cdots, e_j, \cdots, g_N\rangle \tag{1}$$

where $\mathbf{k}$ and $\mathbf{r}_j$ are the wavevector of EM mode and position of the jth TLS, respectively. Equation 1 describes the cooperative nature which has been manifested by the superradiance in a collection of atoms. We next consider a group of molecules whose vibational modes, instead of TLS's, coupled to the electric field in a single-mode infrared cavity, where the solvent causes frequency fluctuation on each molecule. To this end, one can consider the following molecular vibrational Hamiltonian

$$H_p = \hbar\sum_{j=1}^{N}[(\delta_j + \delta\omega_j\eta_j)|v_j\rangle\langle v_j| + g_j(|v_j\rangle\langle G|a + |G\rangle\langle v_j|a^\dagger)] \tag{2}$$

in the rotating frame of the photons, where a is the annihilation operator for cavity photons. $|v_j\rangle$ is the first vibrational excited-state of the jth molecule and $|G\rangle$ gives the vibrational ground state of this N-molecule system. Notice that the description by eq 2 takes the rational when assuming large anharmonicity. Here, ω_j is the vibrational frequency of the jth molecule. $\delta_j \equiv \omega_j - \omega_c$ denotes the molecule−cavity detuning and ω_c is the photon frequency. The variable $\eta_j = \frac{1}{2}(1 - \sigma_j^z)$ and σ_j^z, $\sigma_j^\pm$ represent the Pauli matrices operating on the solvent coordinate at the jth molecule: $\sigma_j^+|q_j\rangle = \sqrt{1 - q_j}|1 - q_j\rangle$, $\sigma_j^-|q_j\rangle = \sqrt{q_j}|1 - q_j\rangle$, $\sigma_j^z|q_j\rangle = (1 - 2q_j)|q_j\rangle$. The terms in eq 2 proportional to η_j give rise to the dynamical disorder via an extra term to the excitation frequency: $\omega_j \rightarrow \omega_j + \Delta\omega(\{q_l\})$ associated with a distribution $P(\{q_l\},t)$ of the collective coordinates q_l describing the motion of solvent molecules. Here we assume a single coordinate q and the two-state description for solvent motion: $q = 0, 1$. The remaining solvent degrees of freedom act as a thermal bath leading to the random transition between these states. The dynamics of the hybrid system including the dynamical disorder is described by Quantum Stochastic Liouville Equation (QSLE): $\dot{\rho} = \frac{i}{\hbar}[\rho, H_p] + \hat{\mathrm{W}}\rho$ with[44,45]

$$\hat{\mathrm{W}}\rho = \sum_{i=1}^{N}\frac{\gamma_i}{2}[\bar{n}_{\nu_i}(\sigma_i^+\rho\sigma_i^- - \sigma_i^-\sigma_i^+\rho) + (\bar{n}_{\nu_i} + 1) \times (\sigma_i^-\rho\sigma_i^+ - \sigma_i^+\sigma_i^-\rho)] + \frac{\omega_c}{2Q}(a\rho a^\dagger - a^\dagger a\rho) + \text{h. c.} \tag{3}$$

describing the dissipation of both vibrations and solvent motion. Here, ν_i is the typical frequency of solvent motion surrounding the ith molecule and $\gamma_i = 2\pi\sum_s \lambda_{i,s}^2\delta(\nu_i - \nu_s^{(i)})$ with $\lambda_{i,s}$ being the system-bath coupling. Q is the quality factor of the infrared cavity. We recall that eq 3 can be rigorously derived from the quantum master equation under weak system−bath coupling.[46] The formal solution of QSLE is $|\rho(t)\rangle\rangle = e^{\hat{\mathcal{L}}t}|\rho(0)\rangle\rangle$ when we recast the QSLE in the form $|\dot{\rho}\rangle\rangle = \hat{\mathcal{L}}|\rho\rangle\rangle$. Let q denote the configurations $\{q_1, q_2, \cdots, q_N\}$ of the solvent motion, $|e_{n'}e_n;q\rangle\rangle \equiv |e_{n'}e_n\rangle\rangle \otimes |q,q\rangle\rangle$ and we use e_j to denote the single excitation of the joint vibration/photon system where e_n; $n = 1, 2, \cdots, N$ represents the single excitation of vibrational mode at the nth molecule and e_{N+1} represents the single photon state of the cavity. The Hamiltonian given by eq 2 is block diagonal with respect to solvent configuration $\{q_1, q_2, \cdots, q_N\}$. All molecules, in resonance with photons (0−0 transition depicted in Figure 1b), result in the two superradiant states, termed lower polariton (LP) and upper polariton (UP). This is obtained by diagonalizing the Hamiltonian H_p in $\{0_1, 0_2, \cdots, 0_N\}$ block (see SI). All other modes are dark. Equation 3 describes the disorder-induced coupling between the polariton

DOI: 10.1021/acs.jpclett.9b00979
J. Phys. Chem. Lett. 2019, 10, 4448−4454

and the emitter dark states that erodes the collective nature of the vibrational polaritons. To elucidate this, let us consider the solution of eq 3 under the initial condition $|\rho(0)\rangle\rangle = |\psi_\alpha^{(J)}, \psi_\alpha^{(J)}\rangle\rangle$. In coordinate space, we find $\rho(x, x'; t) = \langle\langle x, x'|\rho(t)\rangle\rangle$, resulting in

$$\rho(x, x'; t) = \sum_{i,j=1}^{N+1}\sum_{k,l=1}^{N+1}\sum_{q}\sum_{u=1}^{\dim} \chi_{\langle e_i e_j, q\rangle; u} e^{\nu_u t} \chi^{-1}_{u;\langle e_k e_l, J\rangle} C^{(J),*}_{e_k,\alpha} C^{(J)}_{e_l,\alpha} \varphi(x - a_i)\varphi^*(x' - a_j) \quad (4)$$

where $\varphi(x - a_i) = (2/l_i^3\sqrt{\pi})^{1/2}\,(x - a_i)e^{-(x-a_i)^2/2l_i^2}$ is the wave function of the single vibrational excitation at the ith molecule, and χ denotes the similarity matrix diagonalizing the Liouvillian $\mathcal{L}$. The ith molecule is located at position a_i and l_i is the typical length of the vibrational wave function at the ith molecule. ν_n's are the eigenvalues of Liouvillian $\hat{\mathcal{L}}$ with negative real part and dim $= (N + 1)^2 2^N$. Here $C^{(J)}_{el,\alpha}$ is the element of matrix diagonalizing H_p. $\rho(x, x, t)$ gives the spatial density of vibrational excitations, while $\rho(x, x', t)$ gives the intermolecular coherence. As $\mathrm{Re}(\nu_n) \le 0$, both density and coherence will decay as time progresses. However, the coherence decays much faster than the diagonal density $\rho(x, x, t)$. This is demonstrated by comparing the top and middle rows of Figure 2. In these simulations, we consider three $W(CO)_6$ molecules placed in an infrared cavity where the joint-vibration/photon system is initially prepared at UP or an EDS, with strong disorder such that the vibration−photon interaction g_j (j = 1, 2, ···, N) is weaker than the fluctuation of vibrational frequencies, i.e., $g_j < \delta\omega_j$. The disorder that dilutes the intermolecular coherence erodes the collective nature of the vibrational polaritons, resulting in the EDSs weakly coupled to cavity photons.[47] Thus, the excitation transfer between polariton and EDSs shows up, revealed by polariton dynamics in Figure 2c and 2f. Besides, the transfer between different polariton branches shown in Figure 2c and 2f takes place more slowly than the polariton−EDS transfer. This can be neatly understood through Fermi's golden rule of the transition rate $\Gamma_{i\to f} = \frac{2\pi}{\hbar}|\langle f|V|i\rangle|^2 \mathcal{N}_i \mathcal{D}_f$ by noting that there are a larger number of EDSs than polaritons. There are $(N + 1)2^N - 2 = 30$ emitter dark states for $N = 3$ where 7 of them with nonvanishing dipole moments are plotted by the solid curves in Figure 2c and 2f. This is because these dark states will become visible in spectroscopic signals. Later on, we will develop a coherent 2D-infrared spectroscopy to monitor the coupling between the polaritons and EDSs.

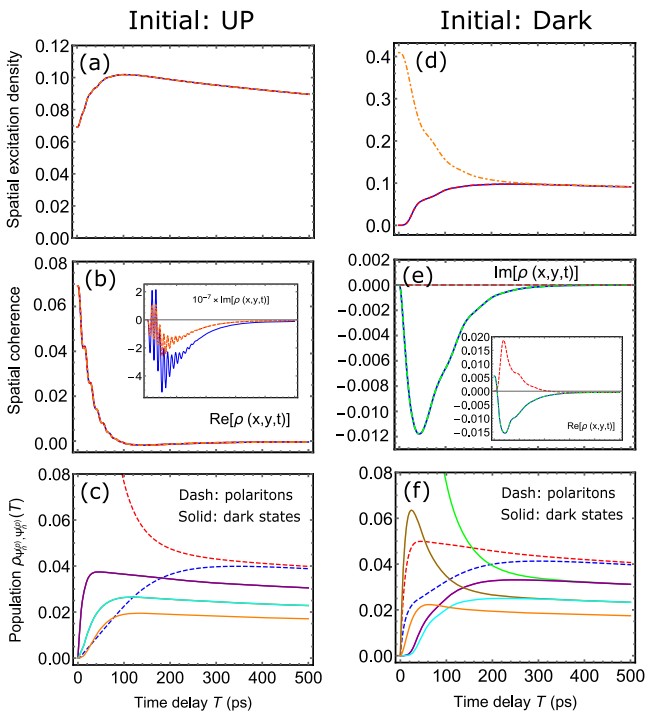

Figure 2. Time-evolution of the density matrix of three $W(CO)_6$ molecules placed along the axis of infrared cavity. (Top) Population of the excitations at individual molecule; (Middle) Intermolecular coherence; (Bottom) Polariton populations. In the bottom row, dashed blue and dashed red lines correspond to lower polariton (LP) and upper polariton (UP), respectively; Solid lines (green, magenta, yellow, purple, brown, cyan, orange) in the bottom row correspond to those emitter dark modes with nonvanishing dipole that may be visible in spectroscopic signals. Molecular parameters are ω_j = 1983 cm^{-1}, ω_c = 1983 cm^{-1}, $\delta\omega_j$ = 18 cm^{-1}, g_j = 2.1 cm^{-1}, ν_j = 62 cm^{-1}, γ_j = 0.18 cm^{-1}, ω_c/Q = 0.04 cm^{-1}, and T = 300 K.

The faster decay of intermolecular coherence than the populations, shown in Figure 2a and 2b, may imply the excitation of the joint vibration/photon system localized in the vicinity of the individual molecule, whereas the polariton mode waves extended over the whole material. The localized state results from a certain coherent superposition of several eigenmodes of the hybrid system.

In the following, we consider coherent 2D-IR spectroscopy for the joint vibration/photon systems incorporating the disorder effect. The system interacts with three temporally well separated pulses through dipolar coupling

$$U = -\sum_{j=1}^{3} \mu^{(j),+} E(t - \tau_j) e^{i\mathbf{k}_j\cdot\mathbf{r}} - \text{h. c.}$$

where $\mu^{(j),+}(t) = \boldsymbol{\mu}^+(t)\cdot\mathbf{e}_j$, $\mathbf{e}_j$ is the unit polarization vector of the jth pulse, and $E(t - \tau_j)$ is the pulse shape whose frequency-domain counterpart is assumed to be Gaussian, i.e., $\tilde{E}(\omega - \nu_j) = E_0^{(j)} \exp[-(\omega - \nu_j)^2/2\sigma_j^2]$. The photon-echo signal is collected along the direction $\mathbf{k}_s = -\mathbf{k}_1 + \mathbf{k}_2 + \mathbf{k}_3$ and interfer with the fourth pulse (local oscillator). This results in the heterodyne-detected signal $\mathrm{Im}(\langle\boldsymbol{\mu}^{lo,-}\rangle\cdot\mathbf{E}_{lo}^*)$. The three controllable time delays are defined as $T_1 = \tau_2 - \tau_1$, $T_2 = \tau_3 - \tau_2$, and $T_3 = \tau_{lo} - \tau_3$. Fourier transform with respect to T_1 and T_3 gives the signal

$$\begin{aligned} S_I(\Omega_3, T_2, \Omega_1) = \frac{8\pi^3}{\hbar^3 V}\int_0^\infty dT_3\int_0^\infty dT_1\int_{-\infty}^\infty dt\int_0^\infty dt_3\int_0^\infty dt_2 \\ \times \int_0^\infty dt_1 e^{i(\Omega_3 T_3 + \Omega_1 T_1)} R^{(3)}(t_3, t_2, t_1) E_{lo}^*(t - \tau) \\ \times E_3(t - t_3 - \tau_3) E_2(t - t_3 - t_2 - \tau_2) \\ \times E_1^*(t - t_3 - t_2 - t_1 - \tau_1) \end{aligned} \quad (5)$$

and the dynamical information on molecules is contained in the third-order response function $R^{(3)}(t_3, t_2, t_1) = R_1(t_3, t_2, t_1) + R_2(t_3, t_2, t_1) - R_3(t_3, t_2, t_1)$ where

DOI: 10.1021/acs.jpclett.9b00979
J. Phys. Chem. Lett. 2019, 10, 4448−4454

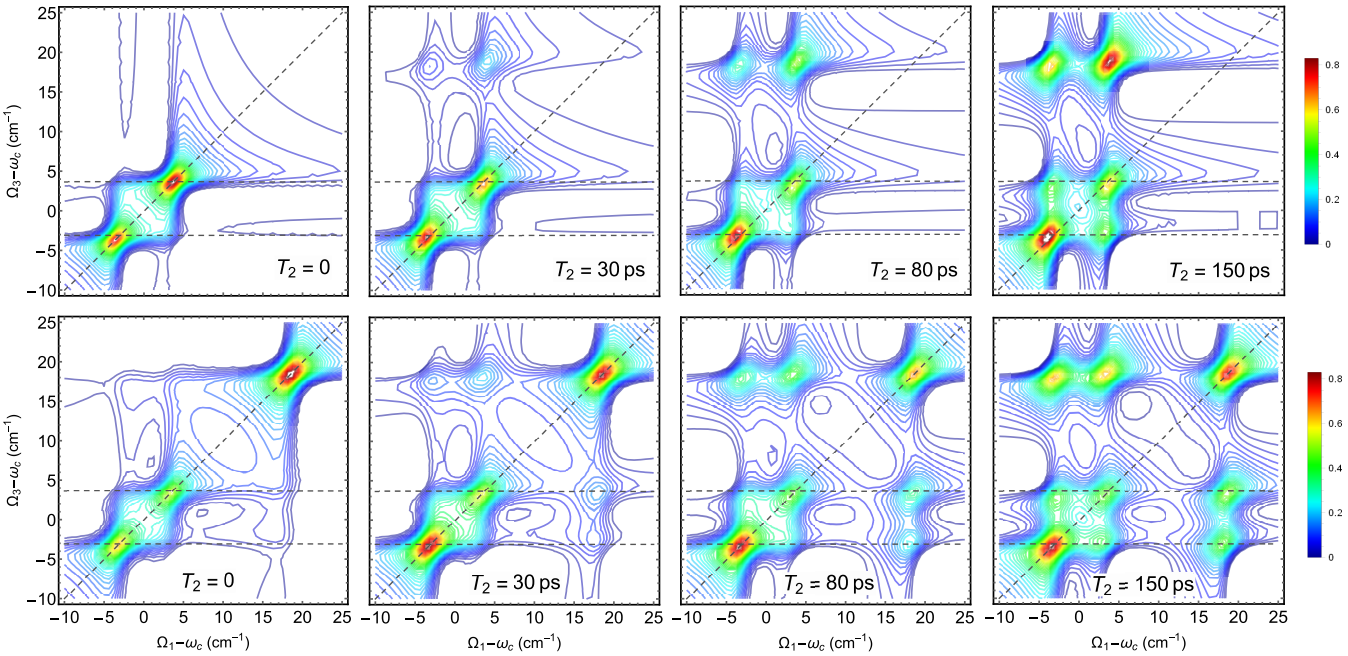

Figure 3. 2D-IR signal variation with T_2 delay, given by eq 5, for three $W(CO)_6$ molecules placed in an infrared microcavity with a linear fashion along the cavity axis. Prior to pulse action, (top) the solvent motion is not considered and (bottom) the solvent is at thermal equilibrium under room temperature. Ω_1 and Ω_3 correspond to excitation and emission frequencies, respectively. Molecular parameters are the same as in Figure 2. Pulse shape is set to be Gaussian with the parameters $\sigma_1 = \sigma_2 = \sigma_3 = \sigma_{lo} = 50$ cm^{-1}, $\omega_1 = \omega_2 = 1983$ cm^{-1}, and $\omega_3 = \omega_{lo} = 1993$ cm^{-1}.

$$R_1(t_3, t_2, t_1) = \sum_q P_q \langle\langle 1|\mu_L^{(lo),-}\mathcal{G}(t_3)\mu_R^{(3),+}\mathcal{G}(t_2)\mu_L^{(2),+}\mathcal{G}(t_1)\mu_R^{(1),-}|G^{(q)}, G^{(q)}\rangle\rangle$$

$$R_2(t_3, t_2, t_1) = \sum_q P_q \langle\langle 1|\mu_L^{(lo),-}\mathcal{G}(t_3)\mu_L^{(3),+}\mathcal{G}(t_2)\mu_R^{(2),+}\mathcal{G}(t_1)\mu_R^{(1),-}|G^{(q)}, G^{(q)}\rangle\rangle$$

$$R_3(t_3, t_2, t_1) = \sum_q P_q \langle\langle 1|\mu_L^{(lo),-}\mathcal{G}(t_3)\mu_L^{(3),+}\mathcal{G}(t_2)\mu_L^{(2),+}\mathcal{G}(t_1)\mu_R^{(1),-}|G^{(q)}, G^{(q)}\rangle\rangle \quad (6)$$

R_1 and R_3 correspond to the excited-state relaxation (ESR) and excited-state decay (ESD), respectively, as depicted by the Feynman diagrams in Figure S1 in SI. Here the ESD refers to the de-excitation of the system from vibrationally excited states back to ground state, which is caused by cavity leakage. The subscripts L,R denote the operations from left and right sides, respectively. That is $A_L|\rho\rangle\rangle = |A\rho\rangle\rangle$, $A_R|\rho\rangle\rangle = |\rho A\rangle\rangle$. Here, $\mathcal{G}(t)$ represents the free propagator of molecules, governed by eq 3. In our model, the R_2 describes the solvent relaxation itself, which has nothing to do with the vibrational polaritons. P_q denotes the statistical probability associated with $|G^{(q)}\rangle$. At thermal equilibrium,

$$P_q = 2^{-N}\prod_{s=1}^{N}\left[1 + (-1)^{\delta_{q_s,1}}\tanh\left(\frac{\hbar v_s}{2k_BT}\right)\right] \quad (7)$$

In general, calculating the signal in eq 5 is hard, due to the integrals over pulse shapes. To simplify the calculations we invoke the *impulsive approximation*[48−50] where the pulse is short compared with the dephasing and solvent time scales. Inserting eq 3 into $R^{(3)}(t_3, t_2, t_1)$ and carrying out the multifold convolutions with respect to pulse envelopes, we can compute the 2DIR signal via some tedious algebra which we will not reproduce here.

To reveal the effect of disorder, we first neglect the thermal excitations of the solvent before the interaction with pulses. Thermal excitations of the solvent will be taken into account later. The top row in Figure 3 shows the tomographies of 2D-IR signal $\mathrm{Im}[S_I(\Omega_3, T_2, \Omega_1)]$ with various T_2 delays. We first note that the line-broadening along the diagonal is larger than that along the anti-diagonal. This is reasonable because of the inhomogeneous broadening attributed to the solvent. As T_2 is varied, the cross peaks above the diagonal show up and their intensities keep increasing. Cross peaks with $\Omega_1 - \omega_c \simeq 3.6$ cm^{-1} ($\Omega_1 - \omega_c \simeq -3.6$ cm^{-1}) and $\Omega_3 - \omega_c \simeq 18$ cm^{-1} manifest the excitation transfer from UP (LP) to EDSs weakly coupled to cavity modes. This is elucidated by the fixed probe frequency Ω_3 without much shift as T_2 increases. Besides, the cross peak positioned at $\Omega_1 - \omega_c \simeq 3.6$ cm^{-1} and $\Omega_3 - \omega_c \simeq -3.6$ cm^{-1} indicates excitation transfer from UP to LP, while the cross peak at $\Omega_1 - \omega_c \simeq -3.6$ cm^{-1} and $\Omega_3 - \omega_c \simeq 3.6$ cm^{-1} indicates excitation transfer from LP to UP. Lower peak intensity at $\Omega_1 - \omega_c \simeq \pm 3.6$ cm^{-1} and $\Omega_3 - \omega_c \simeq \mp 3.6$ cm^{-1} than the one at $\Omega_1 - \omega_c \simeq \pm 3.6$ cm^{-1} and $\Omega_3 - \omega_c \simeq 18$ cm^{-1} implies the system of interest is more in favor of populating EDSs than populating polaritonic states. We can further observe from these peak variations that the polariton−polariton transfer occurring in ∼100 ps is slower than the ∼30 ps polariton-EDS transfer. This is supported by the population dynamics depicted in Figure 2c. Moreover, the top row of Figure 3 illustrates that the rate of UP → EDSs is higher than that of LP → EDSs. This is consistent with the time evolution of both populations and intermolecular coherence obtained before.

In the bottom row of Figure 3, we plot the 2D-IR signal $\mathrm{Im}[S_I(\Omega_3, T_2, \Omega_1)]$ for various T_2 delays, by including thermal excitations of the solvent whereas the molecules are in the

DOI: 10.1021/acs.jpclett.9b00979
J. Phys. Chem. Lett. 2019, 10, 4448−4454

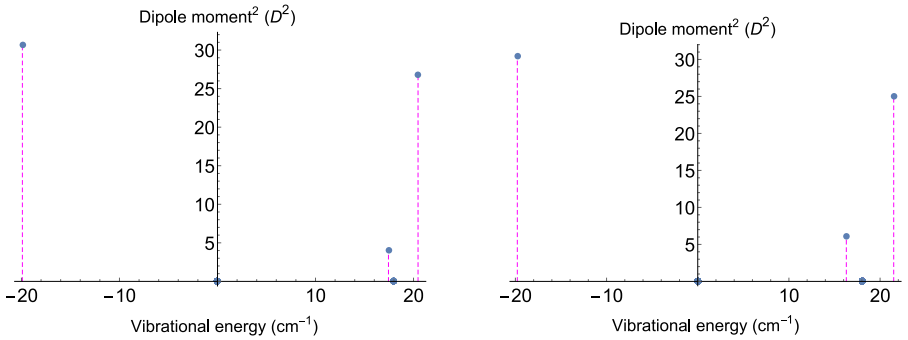

Figure 4. Dipole moment strength varies with energy levels of the joint vibration/photon system, for 4137 $W(CO)_6$ molecules placed in an IR cavity with a linear fashion along the cavity axis. (Left) 30 and (right) 130 out of 4137 $W(CO)_6$ molecules are large-detuned to cavity photons. $g_j\sqrt{N} = 19\text{cm}^{-1}$ and $N = 4137$.[42] Other molecular parameters are the same as Figure 2.

vibrational ground state prior to the pulse actions. Compared to the top row, we now observe cross peaks both above and below the diagonal line. In addition to the information given by the top row of Figure 3, an extra peak positioned at $\Omega_1 - \omega_c = \Omega_3 - \omega_c \simeq 18\ \text{cm}^{-1}$ can be observed even at $T_2 = 0$. This indicates that the thermal motion of the solvent may make the EDSs visible in absorption spectra, manifesting the modifications of the polaritonic structure of molecular vibrations. The excitation transfer from EDSs to UP (LP) is further evident by the cross peaks at $\Omega_1 - \omega_c \simeq 18\ \text{cm}^{-1}$ and $\Omega_3 - \omega_c \simeq 3.6\ \text{cm}^{-1}$ ($\Omega_3 - \omega_c \simeq -3.6\ \text{cm}^{-1}$) below the diagonal, when the EDSs are populated. The population transfer between EDSs and polariton states is faster than that between LP and UP, as evident from the polariton dynamics shown in Figure 2f. So far, the analysis based on Figure 3 clearly elucidates how the cooperativity in the joint vibration/photon system is eroded by the local fluctuations (i.e., disorder), associated with the presence of extra cross peaks other than those characterizing the polariton modes. This allows us to explain and better understand the recent experiments[42] where the coupling between bright polariton and EDSs was demonstrated. However, the positions of EDSs relative to polariton states in 2D-IR spectra predicted by our work shows the deviation from these experiments.[42] This is due to the fewer molecules considered in our simulations (for $N = 3$, $g\sqrt{N} \simeq 3.6\text{cm}^{-1} \ll \delta\omega$) than many experiments which had ∼4000 $W(CO)_6$ molecules in the infrared cavity. To support this, we further calculate the distribution of dipole moments for an ensemble with 4137 $W(CO)_6$ molecules, as depicted in Figure 4, where (left) and (right) correspond to 30 and 130 out of 4137 molecules being large-detuned off cavity frequency under the influence of solvent-induced disorder. The extra peaks sandwiched in between the two polariton branches may be attributed to the EDSs since the associated frequency shift of a few cm^{-1}'s (compare Figure 4(left) and (right)) is much smaller than the Rabi splitting $\simeq 2g\sqrt{N} \simeq 40\text{cm}^{-1}$ between the two polariton branches. Figure 4, combined with Figure 3, thereby helps in understanding the experimental results.[42] Applying eq 3 for large number of molecules will be an interesting future goal.

It is worth noting that recent 2D-IR experiments on vibrational polaritons assumed $\mathbf{k}_1 = \mathbf{k}_2$, which indeed results in the 2D pump−probe scheme.[42] To compensate such a discrepancy, we plot in Figure S4 in SI the 2D pump−probe spectra given the phase matching $\mathbf{k}_s = \mathbf{k}_3$. As shown, all the dynamical information on the system of interest, except the line-broadening mechanism, resolved by the pump−probe scheme is the same as that given by Figure 3. This can be easily understood from the multidimensional spectroscopic theory.[45,48]

In conclusion, we studied the cooperative properties of molecular polaritons, by 2D infrared spectroscopy incorporating the disorder induced by solvent motion. Through the control of time and frequency scales, we demonstrated how the signal captures the polariton dynamics that involves the competition between the photon-mediated long-range coherence and local fluctuations. Our work offers new insights on the subtle time evolution of polaritons observed in recent experiments.[42,51] Understanding the cooperative nature of molecular polaritons is significant for the community to gain more details about the diverse phenomena afforded by the polaritons in complex materials. This knowledge may help in the design of vibrational−polariton photonic devices in the mid-IR regime and in polariton chemistry.

The present work can be extended to a large number of molecules with the solvent motion described by continuous coordinates. This would improve the theory to obtain agreement with experiments. In addition to the infrared polarization, the approach developed here can be further generalized to the optical/UV regime, leading to the polaritonic 2D electronic spectroscopy (2DES)/2D ultraviolet (2DUV) spectroscopy. Taking advantage of the lower cost compared to the full simulation of nuclei wavepacket,[52,53] this approach will help the study of cavity-controlled charge transfer and reaction kinetics.

■ ASSOCIATED CONTENT

Supporting Information

The Supporting Information is available free of charge on the ACS Publications website at DOI: 10.1021/acs.jpclett.9b00979.

Description of the stochastic models used in main text is given in detail and some additional materials like the 2D pump−probe spectroscopy (PDF)

■ AUTHOR INFORMATION

Corresponding Authors

*E-mail: zhedong.zhang@tamu.edu.
*E-mail: scully@tamu.edu.
*E-mail: smukamel@uci.edu.

ORCID

Zhedong Zhang: 0000-0002-0305-6064

DOI: 10.1021/acs.jpclett.9b00979
J. Phys. Chem. Lett. 2019, 10, 4448−4454

Shaul Mukamel: 0000-0002-6015-3135

Notes

The authors declare no competing financial interest.

■ ACKNOWLEDGMENTS

We gratefully acknowledge the support of the grants Air Force Office of Scientific Research (Award No. FA9550-18-1-0141), Office of Navy Research (Award No. N00014-16-1-3054) and Robert A. Welch Foundation (Grant No. A-1261). M.S.Z. thanks the support of grant King Abdulaziz City for Science and Technology. S.M. gratefully acknowledges the support of grant NSF-CHE-1663822. We also thank A. V. Sokolov, K. E. Dorfman, T. Peng and G. S. Agarwal for the useful discussions.

■ REFERENCES

(1) Nußmann, S.; Murr, K.; Hijlkema, M.; Weber, B.; Kuhn, A.; Rempe, G. Vacuum-Stimulated Cooling of Single Atoms in Three Dimensions. *Nat. Phys.* **2005**, *1*, 122−125.

(2) Kena-Cohen, S.; Forrest, S. R. Room-Temperature Polariton Lasing in an Organic Single-Crystal Microcavity. *Nat. Photonics* **2010**, *4*, 371−375.

(3) Cacciola, A.; Di Stefano, O.; Stassi, R.; Saija, R.; Savasta, S. Ultrastrong Coupling of Plasmons and Excitons in a Nanoshell. *ACS Nano* **2014**, *8*, 11483−11492.

(4) Tsuchimoto, Y.; Nagai, H.; Amano, M.; Bando, K.; Kondo, H. Cavity Polaritons in an Organic Single-Crystalline Rubrene Microcavity. *Appl. Phys. Lett.* **2014**, *104*, 233307−233310.

(5) Aberra Guebrou, S.; Symonds, C.; Homeyer, E.; Plenet, J. C.; Gartstein, Y. N.; Agranovich, V. M.; Bellessa, J. Coherent Emission from a Disordered Organic Semiconductor Induced by Strong Coupling with Surface Plasmons. *Phys. Rev. Lett.* **2012**, *108*, 066401−066405.

(6) Spano, F. C. Optical Microcavities Enhance the Exciton Coherence Length and Eliminate Vibronic Coupling in J-Aggregates. *J. Chem. Phys.* **2015**, *142*, 184707−184718.

(7) Zhang, Z. D.; Wang, J. Origin of Long-Lived Quantum Coherence and Excitation Dynamics in Pigment-Protein Complexes. *Sci. Rep.* **2016**, *6*, 37629−37637.

(8) Zhang, Z. D.; Wang, J. Assistance of Molecular Vibrations on Coherent Energy Transfer in Photosynthesis from the View of a Quantum Heat Engine. *J. Phys. Chem. B* **2015**, *119*, 4662−4667.

(9) Coles, D. M.; Somaschi, N.; Michetti, P.; Clark, C.; Lagoudakis, P. G.; Savvidis, P. G.; Lidzey, D. G. Polariton-Mediated Energy Transfer between Organic Dyes in a Strongly Coupled Optical Microcavity. *Nat. Mater.* **2014**, *13*, 712−719.

(10) Coles, D. M.; Yang, Y.; Wang, Y.; Grant, R. T.; Taylor, R. A.; Saikin, S. K.; Aspuru-Guzik, A.; Lidzey, D. G.; Tang, J. K.-H.; Smith, J. M. Strong Coupling between Chlorosomes of Photosynthetic Bacteria and a Confined Optical Cavity Mode. *Nat. Commun.* **2014**, *5*, 5561−5569.

(11) Zhang, Z. D.; Saurabh, P.; Dorfman, K. E.; Debnath, A.; Mukamel, S. Monitoring Polariton Dynamics in the LHCII Photosynthetic Antenna in a Microcavity by Two-Photon Coincidence Counting. *J. Chem. Phys.* **2018**, *148*, 074302−074314.

(12) Kowalewski, M.; Bennett, K.; Mukamel, S. Cavity Femtochemistry: Manipulating Nonadiabatic Dynamics at Avoided Crossings. *J. Phys. Chem. Lett.* **2016**, *7*, 2050−2054.

(13) Bellessa, J.; Bonnand, C.; Plenet, J. C.; Mugnier, J. Strong Coupling between Surface Plasmons and Excitons in an Organic Semiconductor. *Phys. Rev. Lett.* **2004**, *93*, 036404−036407.

(14) Shalabney, A.; George, J.; Hutchison, J.; Pupillo, G.; Genet, C.; Ebbesen, T. W. Coherent Coupling of Molecular Resonators with a Microcavity Mode. *Nat. Commun.* **2015**, *6*, 5981−5986.

(15) Schwartz, T.; Hutchison, J. A.; Genet, C.; Ebbesen, T. W. Reversible Switching of Ultrastrong Light-Molecule Coupling. *Phys. Rev. Lett.* **2011**, *106*, 196405−196408.

(16) Haroche, S. Cavity Quantum Electrodynamics. *Phys. Today* **1989**, *42*, 24−30.

(17) Raimond, J. M.; Brune, M.; Haroche, S. Manipulating Quantum Entanglement with Atoms and Photons in a Cavity. *Rev. Mod. Phys.* **2001**, *73*, 565−582.

(18) Scully, M. O.; Kocharovsky, V. V.; Belyanin, A.; Fry, E.; Capasso, F. Enhancing Acceleration Radiation from Ground-State Atoms via Cavity Quantum Electrodynamics. *Phys. Rev. Lett.* **2003**, *91*, 243004−243007.

(19) Dicke, R. Coherence in Spontaneous Radiation Processes. *Phys. Rev.* **1954**, *93*, 99−110.

(20) Tavis, M.; Cummings, F. W. Exact Solution for a *N*-Molecule-Radiation-Field Hamiltonian. *Phys. Rev.* **1968**, *170*, 379−384.

(21) Gross, M.; Haroche, S. Superradiance: An Essay on the Theory of Collective Spontaneous Emission. *Phys. Rep.* **1982**, *93*, 301−396.

(22) Scully, M. O.; Fry, E. S.; Raymond Ooi, C. H.; Wodkiewicz, K. Directed Spontaneous Emission from an Extended Ensemble of *N* Atoms: Timing Is Everything. *Phys. Rev. Lett.* **2006**, *96*, 010501−010504.

(23) Scully, M. O.; Svidzinsky, A. A. The Super of Superradiance. *Science* **2009**, *325*, 1510−1511.

(24) Spano, F. C.; Mukamel, S. Superradiance in Molecular Aggregates. *J. Chem. Phys.* **1989**, *91*, 683−700.

(25) Spano, F. C.; Kuklinski, J. R.; Mukamel, S. Temperature-Dependent Superradiant Decay of Excitons in Small Aggregates. *Phys. Rev. Lett.* **1990**, *65*, 211−214.

(26) Lidzey, D. G.; Bradley, D. D. C.; Skolnick, M. S.; Virgili, T.; Walker, S.; Whittaker, D. M. Strong ExcitonPhoton Coupling in an Organic Semiconductor Microcavity. *Nature* **1998**, *395*, 53−55.

(27) Herrera, F.; Spano, F. C. Absorption and Photoluminescence in Organic Cavity QED. *Phys. Rev. A: At., Mol., Opt. Phys.* **2017**, *95*, 053867−053890.

(28) Herrera, F.; Spano, F. C. Cavity-Controlled Chemistry in Molecular Ensembles. *Phys. Rev. Lett.* **2016**, *116*, 238301−238306.

(29) Galego, J.; Garcia-Vidal, F. J.; Feist, J. Cavity-Induced Modifications of Molecular Structure in the Strong-Coupling Regime. *Phys. Rev. X* **2015**, *5*, 041022−041035.

(30) Kowalewski, M.; Bennett, K.; Mukamel, S. Non-Adiabatic Dynamics of Molecules in Optical Cavities. *J. Chem. Phys.* **2016**, *144*, 054309−054316.

(31) Pino, J. d.; Feist, J.; Garcia-Vidal, F. J Quantum Theory of Collective Strong Coupling of Molecular Vibrations with a Microcavity Mode. *New J. Phys.* **2015**, *17*, 053040−053049.

(32) Thomas, A.; George, J.; Shalabney, A.; Dryzhakov, M.; Varma, S. J.; Moran, J.; Chervy, T.; Zhong, X.; Devaux, E.; Genet, C.; et al. Ground-State Chemical Reactivity under Vibrational Coupling to the Vacuum Electromagnetic Field. *Angew. Chem., Int. Ed.* **2016**, *55*, 11462−11466.

(33) Hutchison, J. A.; Schwartz, T.; Genet, C.; Devaux, E.; Ebbesen, T. W. Modifying Chemical Landscapes by Coupling to Vacuum Fields. *Angew. Chem.* **2012**, *124*, 1624−1628.

(34) Zhang, Z. D.; Mukamel, S. Fluorescence Spectroscopy of Vibronic Polaritons of Molecular Aggregates in Optical Microcavities. *Chem. Phys. Lett.* **2017**, *683*, 653−657.

(35) Saurabh, P.; Mukamel, S. Two-Dimensional Infrared Spectroscopy of Vibrational Polaritons of Molecules in an Optical Cavity. *J. Chem. Phys.* **2016**, *144*, 124115−124121.

(36) Tokmakoff, A.; Sauter, B.; Fayer, M. D. Temperature-Dependent Vibrational Relaxation in Polyatomic Liquids: Picosecond Infrared Pump-Probe Experiments. *J. Chem. Phys.* **1994**, *100*, 9035−9043.

(37) Arrivo, S. M.; Dougherty, T. P.; Grubbs, W. T.; Heilweil, E. J. Ultrafast Infrared Spectroscopy of Vibrational CO-Stretch Up-Pumping and Relaxation Dynamics of $W(CO)_6$. *Chem. Phys. Lett.* **1995**, *235*, 247−254.

(38) Wilmer, B. L.; Passmann, F.; Gehl, M.; Khitrova, G.; Bristow, A. D. Multidimensional Coherent Spectroscopy of a Semiconductor Microcavity. *Phys. Rev. B: Condens. Matter Mater. Phys.* **2015**, *91*, 201304−201309.

DOI: 10.1021/acs.jpclett.9b00979
J. Phys. Chem. Lett. 2019, 10, 4448−4454

(39) Albert, F.; Sivalertporn, K.; Kasprzak, J.; Straub, M.; Schneider, C.; Höfling, S.; Kamp, M.; Forchel, A.; Reitzenstein, S.; Muljarov, E. A.; et al. Microcavity Controlled Coupling of Excitonic Qubits. *Nat. Commun.* **2013**, *4*, 1747−1753.
(40) Lomsadze, B.; Cundiff, S. T. Frequency Combs Enable Rapid and High-Resolution Multidimensional Coherent Spectroscopy. *Science* **2017**, *357*, 1389−1391.
(41) Lomsadze, B.; Cundiff, S. T. Frequency-Comb Based Double-Quantum Two-Dimensional Spectrum Identifies Collective Hyperfine Resonances in Atomic Vapor Induced by Dipole-Dipole Interactions. *Phys. Rev. Lett.* **2018**, *120*, 233401−233406.
(42) Xiang, B.; Ribeiro, R. F.; Dunkelberger, A. D.; Wang, J.; Li, Y.; Simpkins, B. S.; Owrutsky, J. C.; Yuen-Zhou, J.; Xiong, W. Two-Dimensional Infrared Spectroscopy of Vibrational Polaritons. *Proc. Natl. Acad. Sci. U. S. A.* **2018**, *115*, 4845−4850.
(43) Ribeiro, R. F.; Dunkelberger, A. D.; Xiang, B.; Xiong, W.; Simpkins, B. S.; Owrutsky, J. C.; Yuen-Zhou, J. Theory for Nonlinear Spectroscopy of Vibrational Polaritons. *J. Phys. Chem. Lett.* **2018**, *9*, 3766−3771.
(44) Tanimura, Y. Stochastic Liouville, Langevin, FokkerPlanck, and Master Equation Approaches to Quantum Dissipative Systems. *J. Phys. Soc. Jpn.* **2006**, *75*, 082001−082039.
(45) Abramavicius, D.; Palmieri, B.; Voronine, D. V.; Sanda, F.; Mukamel, S. Coherent Multidimensional Optical Spectroscopy of Excitons in Molecular Aggregates; Quasiparticle versus Supermolecule Perspectives. *Chem. Rev.* **2009**, *109*, 2350−2408.
(46) Scully, M. O.; Zubairy, M. S. *Quantum Optics*; Cambridge University Press: Cambridge, U.K., 1997.
(47) Houdré, R.; Stanley, R. P.; Ilegems, M. Vacuum-Field Rabi Splitting in the Presence of Inhomogeneous Broadening: Resolution of a Homogeneous Linewidth in an Inhomogeneously Broadened System. *Phys. Rev. A: At., Mol., Opt. Phys.* **1996**, *53*, 2711−2715.
(48) Mukamel, S. *Principles of Nonlinear Optical Spectroscopy*; Oxford University Press: New York, U.S.A., 1995.
(49) Yan, Y. J.; Mukamel, S. Femtosecond Pump-Probe Spectroscopy of Polyatomic Molecules in Condensed Phase. *Phys. Rev. A: At., Mol., Opt. Phys.* **1990**, *41*, 6485−6504.
(50) Yan, Y. J.; Mukamel, S. Photon Echoes of Polyatomic Molecules in Condensed Phases. *J. Chem. Phys.* **1991**, *94*, 179−190.
(51) Dunkelberger, A. D.; Spann, B. T.; Fears, K. P.; Simpkins, B. S.; Owrutsky, J. C. Modified Relaxation Dynamics and Coherent Energy Exchange in Coupled Vibration-Cavity Polaritons. *Nat. Commun.* **2016**, *7*, 13504−13513.
(52) Agarwalla, B. K.; Ando, H.; Dorfman, K. E.; Mukamel, S. Stochastic Liouville Equations for Femtosecond Stimulated Raman Spectroscopy. *J. Chem. Phys.* **2015**, *142*, 024115−024124.
(53) Sanda, F.; Mukamel, S. Stochastic Liouville Equations for Coherent Multidimensional Spectroscopy of Excitons. *J. Phys. Chem. B* **2008**, *112*, 14212−14220.

DOI: 10.1021/acs.jpclett.9b00979
J. Phys. Chem. Lett. 2019, 10, 4448−4454